IIETA International Information and Engineering Technology Association
Advancing the World of Information and Engineering

Traitement du Signal
Vol. 43, No. 2, April, 2026, pp. 599-614
Journal homepage: http://iieta.org/journals/ts

Comparative Analysis of Deep Transfer Learning Models for COVID-19 Diagnosis in Computed Tomography Scans

Hammam Alshazly[1,2*], Abdelrahman Abdelnazeer[1], Emad Ahmed[1], Ragaa Ahmed[3], Hela Elmannai[4], Abeer D. Algarni[4]

[1] Department of Computer Science, Faculty of Computers and Information, Qena University, Qena 83523, Egypt
[2] Technology Department, College of Technology and Business, Riyadh Elm University, Riyadh 12734, Saudi Arabia
[3] Mathematics Department, Faculty of Science, Qena University, Qena 83523, Egypt
[4] Department of Information Technology, College of Computer and Information Sciences, Princess Nourah bint Abdulrahman University, Riyadh 11671, Saudi Arabia

Corresponding Author Email: ha.alshazly@svu.edu.eg

https://doi.org/10.18280/ts.430204

Received: 25 September 2025
Revised: 6 December 2025
Accepted: 15 December 2025
Available online: 30 April 2026

Keywords:
COVID-19 detection, deep learning, activation function, transfer learning, performance evaluation, fine-tuning

ABSTRACT

The emergence of the novel coronavirus, SARS-CoV-2, has led to a highly contagious disease, COVID-19, which has evolved into a global health catastrophe. The rapid and widespread transmission of the virus has created significant challenges for its early and accurate detection. In response, deep learning (DL) methods, specifically transfer learning, have demonstrated promising capabilities in medical image analysis and are thus being explored as a potential tool for the accurate diagnosis of COVID-19 using Computed Tomography (CT) scans. This research presents a transfer learning methodology for detecting COVID-19 CTs. The approach leverages pre-trained Convolutional Neural Networks (CNNs) and evaluates the effectiveness of several deep network architectures, including DenseNet121, DenseNet201, Xception, InceptionV3, MobileNetV2, MobileNet, ResNet152V2, and ResNet101v2. The architectures are fine-tuned on a large dataset of CT imaging made up of three distinct categories, including positive CT (pCT), non-informative CT (NiCT), and negative CT (nCT). To evaluate the performance of the proposed approaches, several experiments are carried out using various performance metrics. The proposed models achieve accuracy, recall, F1-score, and precision values above 99%, which shows a potential and automated tool for CT scan-based COVID-19 identification. Moreover, we applied different activation functions for some specific models to improve their detection performance. The results demonstrated a modest yet meaningful improvement of approximately 2% across all performance metrics for certain models. To better interpret these results, a visualization technique was employed to highlight the discriminative regions that primarily contributed to the model's predictions.

1. INTRODUCTION

Coronavirus Disease 2019 (COVID-19) is classified as a disease caused by a novel coronavirus designated as SARS-CoV-2. The virus indicated is the key cause of the COVID-19 pandemic [1]. This viral pathogen exhibits a remarkably high level of contagiousness, facilitating its rapid transmission among individuals primarily through respiratory droplets. These tiny droplets, released during actions including sneezing, speaking, or coughing by an infected person, operate as carriers of the virus and may be inhaled by others at a short distance. Moreover, indirect transmission may transpire via contact with infected surfaces or things that have been handled by patients. Consequently, adopting stringent hygiene practices, employing facial masks, adhering to physical distancing protocols, and adhering to other recommended public health interventions are of paramount importance in curbing the dissemination of the virus.

There are several methods for detecting COVID-19, but the most common ones are RT-PCR testing and Computed Tomographys (CTs). The RT-PCR test involves the collection of a patients nasal or throat sample, which is subsequently analyzed to detect the presence of viral genetic material. This test has served as the benchmark diagnostic method for detecting COVID-19. It has become well-known for being accurate and dependable at finding the virus. However, it may take several days to get the test results, and false negatives can happen if the sample is not collected properly or if the virus is not found in the sample.

CT scans provide an alternative approach for COVID-19 diagnosis, allowing the visualization of lung abnormalities associated with the disease. CT scans offer rapid results but are less specific than RT-PCR testing and may yield false positives in certain cases. It is essential to depend on the knowledge provided by medical experts to ascertain the most suitable diagnostic method based on particular circumstances and clinical indications. Conversely, CT scans are a medical imaging modality that produces high-resolution, three-

dimensional representations of the inside architecture of the human body. Regarding COVID-19, CTs may evaluate the virus's effects on the patient's lungs and allow for ground-glass opacities or lung consolidation, both of which are prevalent indicators of pneumonia resulting from COVID-19. The effectiveness of CT imaging for COVID-19 diagnosis lies in its ability to rapidly produce detailed images of the lung parenchyma, which can reveal characteristic radiographic patterns associated with viral pneumonia. This technology makes CT scans a vital tool for doctors in emergency situations, as imaging results can be obtained within minutes. Therefore, CT scans can provide an alternative approach for COVID-19 diagnosis, allowing the visualization of lung abnormalities associated with the disease. However, it is essential to know that CTs are not as reliable as RT-PCR testing, which directly identifies the presence of the SARS-CoV-2 virus. CT scans can produce false-positive results if the patient has other underlying lung abnormalities or diseases, as the imaging findings may not be specific to COVID-19. Consequently, the selection of a diagnostic method often relies on the particular clinical context and the urgency of acquiring the data. A combination of CTs and RT-PCR tests may be used to provide a more thorough diagnosis of COVID-19 infection. The rapid proliferation of the COVID-19 pandemic has demanded the development of effective diagnostic techniques to aid in the early and timely identification and treatment of the virus. In this regard, researchers have investigated the utilization of Convolutional Neural Networks (CNNs), a category of deep learning (DL) algorithms.

CNNs have the potential to automate the analysis of CT scans, enabling faster and more accurate diagnoses of COVID-19. These methods for DL on extensive datasets of labelled CT images enable them to identify the unique characteristics of COVID-19 pneumonia and distinguish it from other lung diseases. While the use of CNNs for COVID-19 diagnosis from CT scans is a promising approach, it is still in the early stages of development and implementation. However, CNNs require large and diverse datasets of labeled images to train effectively, and their performance is heavily dependent on the quality and representativeness of the training data. Therefore, alternative techniques, such as transfer learning (TL) strategies from previously validated deep networks along with data augmentation techniques, may be necessary to address the limitations of the current CNN-based approaches [2-5].

This paper's primary features are as described below:

- Providing a robust TL technique to modify deep CNN models with several architectural configurations, this approach demonstrates its effectiveness using experimental data. The models were partially fine-tuned to reduce training time and memory consumption.
- Implementing the MobileNet, Inception, DenseNet, ResNet, and Xception frameworks and evaluating their performance using precision, accuracy, recall, and F1 scores. Our models attained very competitive results with an accurate rate of 99%.
- Evaluating the impact of different activation functions on model performance for detecting COVID-19 pneumonia from chest CT scans revealed an improvement of approximately 2% across all performance evaluation metrics.
- Employing the Gradient-weighted Class Activation Mapping (Grad-CAM) technique enhanced the explainability of the models and facilitated the interpretation of their decision-making process.

The following sections of the paper are organized and described as follows. The relevant research conducted in the area of COVID-19 diagnosis and detection is covered in Section 2. The different deep CNN architectures that are assessed in this work are defined in Section 3. In Section 4, the proposed model, CT scan dataset, and model selection strategies are explained. Section 5 describes the experimental results. The conclusions, along with potential for future research, are presented in Section 6.

2. RELATED WORK

COVID-19 has highlighted the necessity of quick and sensitive diagnostic tools. Where DL has shown improvements in the early identification of COVID-19 with medical imaging techniques, involving chest X-rays and CTs, this section analyses several studies on COVID-19 detection using medical imaging and CNN approaches.

Zheng et al. [6] devised a DL algorithm capable of identifying COVID-19 cases from chest CTs. A dataset comprising CT scans from individuals diagnosed with COVID-19, viral pneumonia, and healthy controls was used to train the DL algorithm. The model achieved a classification accuracy of 86.7% for COVID-19 cases.

A blockchain-based federated learning method for COVID-19 recognition using CTs was introduced by Kumar et al. [7]. To deal with the variety of CT data gathered from various institutions and scanners, the authors developed a data normalization technique. They then segmented and categorized COVID-19 patients using CTs using a Capsule Network. The dataset used (28,395 out of 34,006) related to patients with COVID-19. With 98% accuracy, the results showed an increased performance in analyzing COVID-19 patients.

Rohila et al. [8] presented an automated DL approach, called ReCOV-101, for analyzing COVID-19 infection using chest CT scans. In order to enhance the classification accuracy, the CTs are preprocessed using segmentation and interpolation techniques. Experiments were carried out for the MosMedData dataset, which comprises CTs for 1110 patients, distributed into five different classes. The implemented model attained an accuracy score of 94.9% for diagnosing COVID-19 in the CTs.

Song et al. [9] introduced an approach for fine-tuning CNNs to classify COVID-19 CT scans. In their framework, a 3D CNN was applied to extract volumetric features from the CT images, resulting in an accuracy of 92.4%. Alshazly et al. [2] explored different deep CNN approaches for classifying COVID-19 in CTs. Two small-sized CT image datasets were used for conducting experiments and evaluating the models.

Alshazly et al. [10] proposed two deep architectures, namely CovidResNet and CovidDenseNet, for identifying COVID-19 using CTs. The experiments were performed using a database of CTs that are classified into three categories. The proposed models were considered for multi-class and binary classification tasks. The best results were achieved for binary classification, achieving an accuracy of 93.87%. Wang et al. [11] introduced a DL-based method for the identification of COVID-19 with the aid of CTs. They used a hybrid 3D and 2D CNN for feature abstraction from the CT images and achieved a 96.5% accuracy.

Li et al. [12] introduced a methodology DL for COVID-19 detection using both CTs and chest X-rays. They used a 2D CNN to extract distinct features for images and obtained an

accuracy rate of 90.8%. An ensemble of DL models was suggested by Kini et al. [13] for the purpose of screening suspicious COVID-19 cases. To enhance the overall detection performance, three pretrained deep models were combined. According to the experimental findings, the suggested ensemble produced an accuracy of 98.98%. Using chest CT scans, Apostolopoulos and Mpesiana [4] created a DL system for COVID-19 identification. Features were extracted from the CT images using a 2D CNN, achieving an accuracy of 95.5%. Hamza et al. [14] introduced a unique framework that combines CNN-LSTM architecture with a feature optimization technique for COVID-19 classification from X-ray. Three publicly accessible datasets were applied in the experiments. The proposed method yields classification results with an accuracy above 93%.

Akl et al. [15] established a CNN-ML ensembled methodology for COVID-19 classification. They used the SARS-CoV-2 CTs database, which consists of a total of 2482 CTs. The dataset contains 2482 positive and negative CT images. They evaluated the effectiveness of feature extraction using a custom CNN and compared it with traditional methods. Feature extraction is carried out with both Scale-Invariant Feature Transform (SIFT) [16] and the proposed CNN model. Classification is performed with a bagging ensemble method to achieve the best accuracy rate of 99.39%.

Kanjanasurat et al. [17] presented an ensemble approach combining CNN and RNN for feature extraction and classification, evaluated on a dataset of 16,210 medical images, comprising CT scans and X-rays of COVID-19, pneumonia, and healthy cases [18-20]. The results show that combining a CNN-RNN model delivers the highest performance. The test results show that the CNN-RNN fusion model performs best, with 93.37% accuracy.

Sahin et al. [21] developed an approach for accurately diagnosing COVID-19 using DL techniques based on CTs. They employed the R-CNN approach for classification purposes. They conducted their experiments on a collected dataset comprising 4000 CT images, including images for pneumonia and COVID-19. The obtained results show that the R-CNN model achieves an accuracy score of 93.86%.

Joshi et al. [22] utilized four ensemble CNN models using TL that can detect COVID-19 with CTs, comparing their performance in CNN architectures. These experiments were performed on a database of SARS-COV-2 CTs [23], which consists of 2,477 CT images. Based on the experiments conducted, the best ensemble model, Ensemble DVX, achieved an accuracy of 97.70%, which combined DenseNet169, VGG16, and Xception architectures.

Sejuti and Islam [24] introduced a CNN-KNN ensembled methodology that can detect COVID-19 CTs. It aims to improve classification accuracy by using a DL approach with data augmentation and 5-fold cross-validation to enhance generalization and reduce overfitting. They used the SARS-CoV-2 CTs, which contain 2482 CTs, 1230 of which are COVID-negative and 1252 of which are COVID-19. The hybrid CNN-KNN model is identified as the best approach for classifying COVID-19 and achieved 98.26% accuracy.

Afif et al. [25] introduced DL for the analysis of COVID-19-related findings in CTs, comprising three primary modules: the attention mix, residual convolutional, and context fusion, along with the purpose of enhancing the timely identification of COVID-19 infection. They used the COVID-x-CT dataset [26] for training, validation, and testing, which contains 60,000 CT scans, and achieved an accuracy of 96.23%.

Riyadi et al. [27] investigated the effectiveness of various optimization methods (SGD, Adamax, and AdaGrad) applied to VGG-16 and VGG-19 for detecting COVID-19 using CTs. A dataset of 2,038 CT scan images was used, consisting of 905 images of lungs affected by COVID-19 and 1,133 images of unaffected lungs. Classification is performed with a VGG-16 approach to achieve the best accuracy rate of 94.11%, outperforming all the tested models.

Maurya et al. [28] suggested a DL approach, Super-xDNN, that integrates image segmentation to improve both the performance and interpretability of algorithms for classifying COVID-19. They considered the CTs dataset that comprises 120 patients, with 60 diagnosed with COVID-19 and 60 non-infected. Their findings indicated that the Super-xDNN architecture reached a classification accuracy of 98.3%.

Roy et al. [29] proposed a TL methodology that utilized a concatenation of three pre-trained architectures, InceptionV3, Xception, and ResNext50, to categorize X-ray images. They used a database of lung X-rays separated into three distinct sets [30]. According to the results, the Xception model performed better than the other two models at identifying COVID-19. When all three models were combined, the suggested approach produced 98.44% classification accuracy.

Echtioui and Ayed [31] proposed a methodology for identifying COVID-19 using pre-trained architectures, including ResNet-50 and DenseNet-169. The study utilized a dataset of 15,156 chest X-ray images categorized into pneumonia, COVID-19, and normal classes, with 14,925 images allocated for training and 231 for testing. The experimental results demonstrated that transfer learning is an effective approach for COVID-19 detection, with DenseNet-169 achieving the highest average accuracy of 90.04%.

Agrawal et al. [32] proposed automating COVID-19 recognition using TL, including VGG19, ResNet50, MobileNetV2, InceptionV3, Xception, and DenseNet121. It addresses the challenges of limited testing resources and aims to improve diagnostic accuracy through advanced image classification techniques. Binary categorization and multiple categories describe the challenges associated with COVID-19 imaging. The suggested ResNet50 models obtained accuracy levels of up to 99.20% and 86.13%, respectively.

Madhavi et al. [33] investigated TL approaches for COVID-19 detection from X-ray images aimed to overcome the limitations of conventional testing methods and support early diagnosis. They considered a dataset that consists of 2,000 X-ray images divided into three classes. The VGG-16 model showed the highest classification performance when evaluated for the selected X-ray dataset, with a sensitivity score of 100%. Table 1 presents some prior works that utilize the TL methods alongside the used datasets and the obtained performance.

Deep CNNs demonstrated promising signs in recognizing COVID-19 from CT scans [34-36]. However, these DL-based approaches face several restrictions that must be avoided before they are widely applied in clinical adoption [37-39]. For example, the limitation of relying on high-quality, large, and available CT classification datasets for training. The ability to access and the availability of such comprehensive datasets may be limited in certain healthcare settings, hindering the development and deployment of robust COVID-19 detection models. Moreover, the inability of DL-based techniques for COVID-19 CT scan detection to distinguish between COVID-19 and other lung conditions with comparable CT scan results presents another difficulty. That is why the DL methods should not be used alone, but should be applied with other

accurate diagnostic tools, such as clinical tests and medical history, to ensure an accurate and reliable diagnosis. Additionally, DL-based CT scan solutions for COVID-19 detection are not yet widely adopted in clinical practice, highlighting the need for further studies and clinical trials to develop efficient and practical solutions.

Table 1. Related works overview of DCNN methods for COVID-19 detection

Author	Architecture(s)	Proposed Approach	Dataset Used	Accuracy
Zheng et al. [6]	Custom DL model	DL-based CT classification using weak labels	CT	86.7%
Rohila et al. [8]	ReCOV-101 model	Segmentation + interpolation + DL classifier	CT	94.9%
Song et al. [9]	3D CNN	Fine-tuned 3D CNN for CT feature extraction	CT	92.4%
Li et al. [12]	2D CNN	Feature extraction for CT & CXR	CT + X-ray	90.8%
Apostolopoulos and Mpesiana [4]	2D CNN	Automated CT-based COVID-19 detection	CT	95.5%
Riyadi et al. [27]	VGG-16, VGG-19	Comparison of optimizers for TL	CT	94.11%
Echtioui and Ayed [31]	ResNet-50, DenseNet-169	TL-based classification + added layers	X-ray	90.04%
Agrawal et al. [32]	VGG19, ResNet50, MobileNetV2, InceptionV3, Xception, DenseNet121	TL for binary & multi-class X-ray	X-ray	99.20% binary, 86.13% multi-class

3. DEEP ARCHITECTURES

Deep CNN architecture has revolutionized the field of image classification by extracting high-level features from raw input image data. However, as the depth of these networks increases to tackle more complex tasks, they commonly have the issue of gradients that explode or vanish, which can hinder their training and performance. This section describes advanced deep CNN architectures and how they have been designed differently to increase their feature extraction capability and decrease their computational complexity. In this study, we explore the representational power of top-performing deep CNNs in image recognition, including Inception [40], ResNet [41], DenseNet [42], MobileNet [43], and Xception [44]. The performance of these architectures is evaluated in our experiments for recognizing COVID-19 from CTs.

3.1 Inception

The Inception architecture, developed by researchers at Google in 2014, has been a highly influential DL architecture for computer vision tasks [40]. In order to enhance the model performance, the Inception model introduced the Inception module. The module applies multiple convolutional filters of varying sizes (1×1, 3×3, 5×5) alongside max pooling. Applying these different sizes filters enables the model to extract features of different spatial sizes. The outputs of the parallel convolutions are then concatenated together along the channel dimension. The following network layer then receives the output from the Inception module. Practically, to construct a deeper network, several Inception modules are stacked before performing a pooling operation to reduce spatial size. Moreover, conventional convolutional layers and max pooling layers are utilized to build the overall deep model.

3.2 ResNet

The CNN architecture known as Residual Network (ResNet) was introduced by researchers at Microsoft in the study by He et al. [41]. ResNet solves the vanishing gradient by the Residual Block. The "skip connections" or "shortcut connections" represent the key ideas behind the Residual Block. These connections enable the deep network to learn the residual mapping from the input to the desired output.

The Residual Block consists of two main components. First, identity shortcut connection, which represents the direct connection that maps the input to the output, enabling the deep network to maintain the integrity of the input information, and prevents the vanishing gradient problem. Second, residual mapping, which is a series of convolutional, activation, and normalization layers to learn how to map residuals from input to the correct class.

The key advantages of the ResNet architecture are the ability to scale to extremely deep networks, with some variants reaching hundreds of layers. This allows the network to extract and learn simple and complex features, leading to improved performance on a wide range of image recognition tasks. Moreover, ResNet is available in several variants, including 18, 50, 101, and 152-layer models. In this study, the evaluation was focused on the deeper configurations with 50, 101, and 152 layers.

3.3 DenseNet

The deep network architecture known as Densely Connected Network (DenseNet) was first shown in the study by Huang et al. [42]. Its primary aim is to reduce the limitations that CNNs usually face by increasing the number of skip connections and by reusing previous feature maps. It has complete layer connectivity, allowing information to be reused and avoiding information decay. The Dense Block, the fundamental component of the DenseNet architecture, is made up of layers stacked one on top of the other, with the output of the preceding block being merged with the input of the current block using fully connected concatenation. It also uses Batch Normalization units to improve information flow and network stability. The DenseNet architecture is designed to address the challenges, such as vanishing gradients and shortcut connections in the ResNet model, while having fewer parameters and more efficient learning than other similar neural networks.

The DenseNet model has achieved leading performance across various image recognition and computer vision tasks. Its efficient parameter utilization and ability to reuse features make it a consistently popular choice for applications with limited computational resources.

3.4 MobileNet

The MobileNet deep architecture, developed by Google researchers in the study by Sandler et al. [43]. The main contributions of the MobileNet architecture are the resolution multiplier, width multiplier, and depthwise separable convolution.

MobileNet employs depthwise separable convolutions. When compared to standard convolutions, this drastically lowers the parameter number and model complexity. To reduce the model size and its computational requirements, MobileNet introduced a hyperparameter called the width multiplier, which enables the network's width (number of channels) to be scaled down uniformly at each layer. Similarly, MobileNet introduced a resolution multiplier hyperparameter, which enables adjusting the input image resolution, providing another way to trade off accuracy for efficiency. Therefore, combining depthwise separable convolutions, a width multiplier, and a resolution multiplier makes the MobileNet models very efficient in terms of parameters and required computations.

Different versions of MobileNet are available, including MobileNet (V1, V2, and V3), with more methods that reduce computing costs while improving accuracy. Due to its effective and outstanding performance in a number of applications, we opted to use it in our experiments.

3.5 Xception

The design of an Extreme Inception CNN is called Xception, which is a deep architecture that extends the idea of the Inception module by leveraging depthwise separable convolutions across the entire network [44]. The Xception architecture shares similarities with MobileNet and ResNet architectures. Similar to MobileNet, the model is more effective since the Xception design drastically lowers the number of parameters and computational cost by substituting depthwise separable convolutions for standard convolutions. Similar to ResNet, the Xception architecture incorporates residual connections between the depthwise separable convolution blocks as introduced in ResNet. Residual connections enhance the flow of data and gradient propagation throughout the architecture, allowing the training of very deep Xception models and simplifying optimization. Moreover, the Xception architecture builds on an improved Inception module, where the concatenation of different convolution branches is replaced by a fully separable convolution structure, which enhances the model's efficiency and performance.

The Xception architecture has demonstrated enhanced performance on several computer vision tasks, while preserving a relatively tiny model size and minimal computational challenge compared to other deep CNN architectures.

4. METHODOLOGY

In this section, we present the deep transfer learning approach employed for classifying COVID-19 using chest CT images. The discussion begins with a description of the CT scan dataset and the prevalent preprocessing methodologies. Then, we discuss the model selection and the proposed methodology of transfer learning, along with performance evaluation metrics.

4.1 Data collection

The initial step in developing an automated COVID-19 detection system involves compiling a dataset of CT scans from COVID-19 patients, alongside scans from healthy individuals and patients with other pulmonary conditions. For this work, we use the publicly accessible COVID-19 CTs database [45]. The dataset consists of CT scans for three different classes, including pCT, nCT, and NiCT, obtained from HUST-Union Hospital patients and authorized by the ethics council for use in research. 6000 CT scans are included from the dataset with chest CT images of 2000 NiCT, 2000 nCT, and 2000 pCT patients. Samples of CT scans from each class in the dataset under consideration are shown in Figure 1.

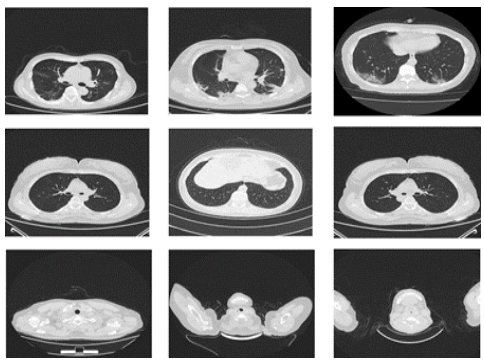

Figure 1. Sample CT scans from the dataset, categorized into three rows: The first row consists of positive CT (pCT) scans diagnosed with COVID-19; the second row contains negative CT (nCT) slices, indicating cases where COVID-19 is not present; the third row shows CT slices with improperly captured lung parenchyma or insufficient data to make a decision

4.2 Data preprocessing

These CT scans have a resolution of 512 × 512 pixels and a depth of 24 bits. All images were downsized to 150 × 150 pixels to match the input size required by the pretrained DL models. In addition to resizing, several preprocessing steps were applied to prepare the images for training. This included intensity normalization to standardize pixel values, channel formatting to ensure compatibility with models pretrained on RGB images, and data augmentation operations such as rotation, flipping, shifting, and zooming to increase variability and reduce. Table 2 summarizes the distribution of CT images across the training and validation sets.

Table 2. The distribution of CT scan samples across the different classes in the dataset

Dataset	Total Images	NiCT	nCT	pCT	Train (60%)	Validation (40%)	Preprocessing
COVID-19 CTs	6000	2000	2000	2000	3600	2400	Resizing to 150 × 150, normalization

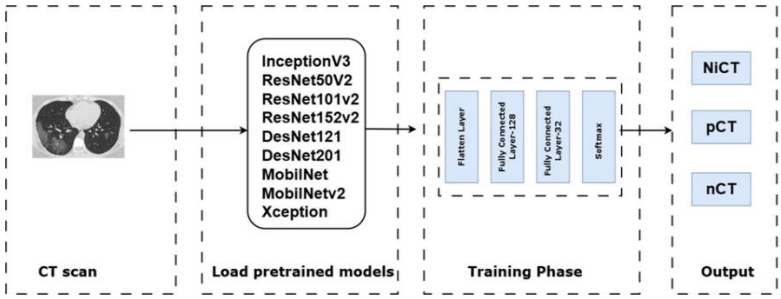

Figure 2. The proposed framework for COVID-19 detection

4.3 Model selection and transfer learning

Figure 2 illustrates the COVID-19 detection framework, which is constructed by leveraging various pre-trained deep CNN architectures. It starts with loading the pre-trained models, where the weights of a pre-trained model are imported. The weights are obtained from a publicly accessible source such as the Keras Applications. This part is essential for initialising the framework with the trained parameters and representations, which serve as a starting point for the fine-tuning process. Then, we replace the original last layer of the pre-trained models with a new set of fully connected layers. We tried various combinations and layers with various numbers of neurons and found that two fully connected layers with 128 and 32 neurons obtain the best results. The last layer comprises a set of neurons, which is equivalent to the number of categories within the specified database. For our COVID-19 dataset, which has three different classes, an output layer with three neurons is attached to enable the classification process.

Throughout the training process, we select specific layers of the pre-trained model that remain frozen, thereby ensuring that key learnt features, including edges, points, and curves, are preserved through these early layers. The learned features serve as a strong foundation for the fine-tuning process, and when we train the customized model using the given COVID-19 dataset. We train the newly added layers to adapt their weights to the specific COVID-19 detection task.

Once we fit the new layers to the new task, we incrementally unfreeze additional layers from the pre-trained model and proceed with the training process. This gradual approach allows the model to build upon the preserved representations in the frozen layers while fine-tuning the newly unfrozen layers. The training is repeated until the model performs as desired on the new dataset and task.

This change aims to ensure that the model is tailored to the COVID-19 classification task on the considered dataset. Notably, the framework utilizes various models such as InceptionV3, ResNet50V2, ResNet101V2, ResNet152, DenseNet121, DenseNet201, MobileNet, MobileNetV2, and Xception.

4.4 Model evaluation and performance metrics

In order to evaluate the performance of the trained models, several evaluation metrics such as accuracy, precision, recall, F1-score, and the confusion matrix are used. To analyze the model's performance and identify any strengths, weaknesses, or potential biases in the model's predictions, we consider the confusion matrix for each model, which provides a summary of the classification results by comparing predicted and actual class labels. The confusion matrix is represented by Table 3 and contains four category values.

Table 3. Confusion matrix for the classification model

	Actual Positive	**Actual Negative**
Predicted Positive	True Positive (TP)	False Positive (FP)
Predicted Negative	False Negative (FN)	True Negative (TN)

Furthermore, to assess the performance of the model applied in classification, the confusion matrix can be used because it contains various metrics, including recall, precision, and F1 score.

$$\text{Accuracy} = \frac{\text{TP} + \text{TN}}{\text{TP} + \text{TN} + \text{FP} + \text{FN}} \quad (1)$$

$$\text{Precision} = \frac{\text{TP}}{\text{TP} + \text{FP}} \quad (2)$$

$$\text{Recall} = \frac{\text{TP}}{\text{TP} + \text{FN}} \quad (3)$$

$$\text{F1} - \text{score} = \frac{2 \times \text{TP}}{2 \times \text{TP} + \text{FP} + \text{FN}} \quad (4)$$

5. EXPERIMENTS AND RESULTS

In this section, we first outline the experimental settings and configure the various deep architecture hyperparameters. Next, we go over the results that were collected and emphasize how well the suggested models work to identify COVID-19 from chest CT images.

5.1 Experimental setup

To build and implement a deep CNN model, we typically follow specific steps that begin with choosing a suitable DL framework. There are different frameworks available, such as TensorFlow, PyTorch, Keras, etc. We utilized Keras and TensorFlow in our experiments. The experiments were conducted on a machine equipped with hardware specifications given in Table 4.

Table 4. The machine specifications for conducting experiments

Parameter	**Value**
Processor	Core(TM) i5-5300U CPU
RAM	8 GB
Hard Disk Drive	500 GB
Operating System	Windows 10
Programming Language	Python
IDE	Jupyter on Google Co-laboratory and Kaggle

5.2 Hyperparameters settings

When utilizing DL algorithms, choosing the right hyperparameters is crucial for determining training parameters and influencing model output. We optimized the networks by choosing particular hyperparameter values for the activation function, batch size, loss function, number of epochs, learning rate, optimizer, and data augmentation qualities in order to attain high accuracy. An overview of the hyperparameters we employed in our investigation is shown in Table 5.

5.3 Results and discussion

We discuss the results of our refined deep networks COVID-19 detection using multi-class data that contains pCT, nCT, and NICT. The loss curves and accuracy curves for each suggested model during the training and validation stages are displayed in Figures 3–11. The training and validation curves represent the models' performance on their respective datasets, illustrating how accuracy and loss evolve throughout the training process. These curves generally show a consistent decline in training loss accompanied by a corresponding increase in training accuracy across the training epochs. Moreover, the training curves show convergence to a low training loss and high training accuracy, which indicates that the models have learned the relevant features and can effectively classify COVID-19 cases in the training data.

The confusion matrix for each model is provided to demonstrate its efficacy in multi-class COVID-19 CT detection. The confusion matrix enables a comprehensive analysis of the model's predictions relative to the actual labels, as illustrated in Figure 12. A detailed analysis and valuable insights to improve a model's performance are provided by the confusion matrix. For instance, the false positives and false negatives in medical research, especially for severe disorders such as COVID-19, must be avoided. Patients with COVID-19 should not be misclassified as negative because false negatives are extremely harmful to society. Moreover, it is crucial to reduce the rate of incorrect diagnoses, namely the misclassification of negative COVID-19 cases as positive.

Table 6 describes information obtained from various deep models: DenseNet201, DenseNet121, Xception, and InceptionV3. The reported evaluation metrics indicate that the accuracy value reaches up to 99% for particular designs, including DenseNet121, Xception, DenseNet201, and InceptionV3. ResNet50V2, which achieved 98% accuracy. The next three models are MobileNet, MobileNetV2, and ResNet152V2, which achieve an accuracy of 97%. The lowest performance is obtained by the ResNet101V2 model, which achieves an accuracy of 96%.

Table 7 presents the results produced from the deep CNN models utilizing various activation functions. Each row indicates a specific model featuring distinct activation functions, along with evaluating performance rates that include precision, recall, accuracy, and F1-score. The models comprise DenseNet121, InceptionV3, MobileNetV2, ResNet152V2, and ResNet101V2, which were all tested with different activation functions that consist of Exponential Linear Unit (ELU) [46], Scaled Exponential Linear Unit (SELU) [47], Rectified Linear Unit (RELU), Leaky RELU [48], Gaussian Error Linear Units (GELU) [49], as well as Parametric Rectified Linear Unit (P RELU) [50].

Table 5. The hyperparameter settings for controlling the training process of various deep Convolutional Neural Network (CNN) models

Training Parameters	InceptionV3	ResNet50V2	ResNet101V2	ResNet152V2	DenseNet121	DenseNet201	MobileNet	MobileNetV2	Xception
Loss-function	categorical_crossentropy								
Rotation range	90	90	90	90	90	90	90	90	90
Optimizer	Adam								
Epochs	100	100	100	100	100	100	100	100	100
Activation function	RELU								
Shear range	0.2	0.2	0.2	0.2	0.2	0.2	0.2	0.2	0.2
featurewise center	True								
Batch size	32	32	32	32	32	32	32	32	32
featurewise normalization	True								
Learning rate	0.0001	0.00001	0.00001	0.0001	0.0001	0.0001	0.00001	0.00001	0.0001
horizontal flip	True								
zoom range	0.2	0.2	0.2	0.2	0.2	0.2	0.2	0.2	0.2

Table 6. The results of the various deep Convolutional Neural Network (CNN) models

Model	Evaluation Metrics			
	Accuracy	Precision	Recall	F1-score
DenseNet121	99	99	99	99
DenseNet201	99	99	99	99
Xception	99	99	99	99
InceptionV3	99	99	99	99
ResNet50V2	98	98	98	98
MobileNet	97	97	97	97
MobileNetV2	97	97	97	97
ResNet152V2	97	97	97	97
ResNet101V2	96	97	96	96

Table 7. The results of the different deep Convolutional Neural Network (CNN) models with varying activation functions

Evaluation Metrics					
Model	**Activation**	**Accuray**	**Precision**	**Recall**	**F1-score**
DenseNet121	ReLU	99	99	99	99
	ELU	99	99	99	99
	SeLU	99	99	99	99
	Leaky ReLU	99	99	99	99
	GeLU	99	99	99	99
	P ReLU	99	99	99	99
InceptionV3	ReLU	99	99	99	99
	ELU	99	99	99	99
	SeLU	99	99	99	99
	Leaky ReLU	99	99	99	99
	GeLU	99	99	99	99
	P ReLU	99	99	99	99
MobileNetV2	ReLU	97	97	97	97
	ELU	99	99	99	99
	SeLU	99	98	98	98
	Leaky ReLU	97	98	97	97
	GeLU	98	98	98	98
	P ReLU	98	98	98	98
ResNet152V2	ReLU	97	97	97	97
	ELU	97	97	97	97
	SeLU	97	97	97	97
	Leaky ReLU	98	98	98	98
	GeLU	98	98	98	98
	P ReLU	98	98	98	98
ResNet101V2	ReLU	96	97	96	96
	ELU	98	98	98	98
	SeLU	98	98	98	98
	Leaky ReLU	98	98	98	98
	GeLU	96	96	96	96
	P ReLU	98	98	98	98

Table 8. The different characteristics and resource consumption of the different deep learning models

Model	Total Params	Size (MB)	Non-Trainable Params	Size (MB)	Trainable Params	Size (MB)	Training Time (s)/Epoch
DenseNet121	9,139,139	(34.86)	6,832,576	(26.06)	2,306,563	(8.80)	21
DenseNet201	22,258,627	(84.91)	18,281,088	(69.74)	3,977,539	(15.17)	24
InceptionV3	24,166,563	(92.19)	21,802,848	(83.17)	2,363,715	(9.02)	21
MobileNet	5,330,499	(20.33)	2,176,256	(8.30)	3,154,243	(12.03)	19
MobileNetV2	6,358,467	(24.26)	1,538,048	(5.87)	4,820,419	(18.39)	22
ResNet50V2	30,122,883	(114.91)	22,510,144	(85.87)	7,612,739	(29.04)	24
ResNet101V2	49,185,699	(187.63)	34,746,944	(132.55)	14,438,755	(55.08)	25
ResNet152V2	64,889,731	(247.53)	57,275,968	(218.49)	7,613,763	(29.04)	35
Xception	27,419,563	(104.60)	16,112,744	(61.47)	11,306,819	(43.13)	23

These findings show that there is generally high performance among all models having scores averaging up to 99% across all performance evaluation metrics. Even though using different activation functions achieved better performance for some models, such as in MobileNetV2 (from 97% using RELU up to 99% using ELU and SELU), ResNet152V2 (from 97% using RELU to 98% using P RELU, GELU, and Leaky RELU), and ResNet101V2 (from 96% using RELU to 98% using PRELU, SELU, ELU, and Leaky RELU). The possible explanations for the slight differences in performance may be attributed to their architecture's variations in the architecture, data splitting, or optimization algorithms used during the training phase. The selection of a suitable activation function matters greatly and depends on the model design and the problem at hand. Activation functions control how signals move through the neural networks and thus affect their performance. The ability of a model to learn from data and generalize it after being trained on specific datasets is determined by the unique properties of each type.

Figure 13, the confusion matrix analysis for the ResNet101V2 model confirms that the observed improvement originates from consistent reductions in misclassification rather than random statistical variation. Activation functions that achieved higher performance, particularly PReLU, SELU, and ELU, demonstrated a noticeable decrease in false negatives, which is critical in the context of COVID-19 diagnosis, along with a slight reduction in false positives. These systematic improvements directly enhanced class-level recall and F1-score, resulting in a stable and reproducible overall gain of approximately 2%. Therefore, the observed enhancement reflects a genuine increase in discriminative capability and overall model robustness, rather than marginal or noise-driven fluctuations.

Finally, the results from Figures 3–13 demonstrate that the proposed deep CNN models achieve a balance between minimizing false negatives, which are critical for patient safety, and controlling false positives, which are important for operational efficiency. The gradual improvements observed

after activation-function tuning indicate increased robustness and suggest that the system can be effectively integrated as a supportive tool alongside RT-PCR testing and radiological evaluation in clinical practice.

Table 8 illustrates the different model characteristics and resource consumption for the different CNN models, such as the total number of parameters, non-trainable and trainable parameters, average training time in seconds per epoch, and size in megabytes (MB). The table shows that the time needed to train the models is proportional to their size.

The models that have many more parameters generally require more training time than smaller models. For instance, ResNet152V2, which is the largest model in size, has the highest training time per epoch. Furthermore, the trainable parameters are directly correlated to the complexity of a model. Large models have higher trainable parameters and are thus more complex. This connection shows that large models can possibly learn to interpret complex patterns, but they will require more computing resources when training.

5.4 Gradient-weighted Class Activation Mapping visualization

To enhance model transparency and facilitate visual interpretation of the results, Grad-CAM localization maps generated by several models are presented. CT scans from the COVID-19 class in the test set were used to highlight the most relevant regions contributing to the predicted outcomes. Figure 14 presents instances of CT images from the COVID-19 CT scan dataset together with their corresponding localization maps. Notably, our DenseNet121 model correctly identified most of the cases as COVID-19 CTs and indicated the areas of defect in the CTs, which is important for evaluating the DenseNet121 architecture.

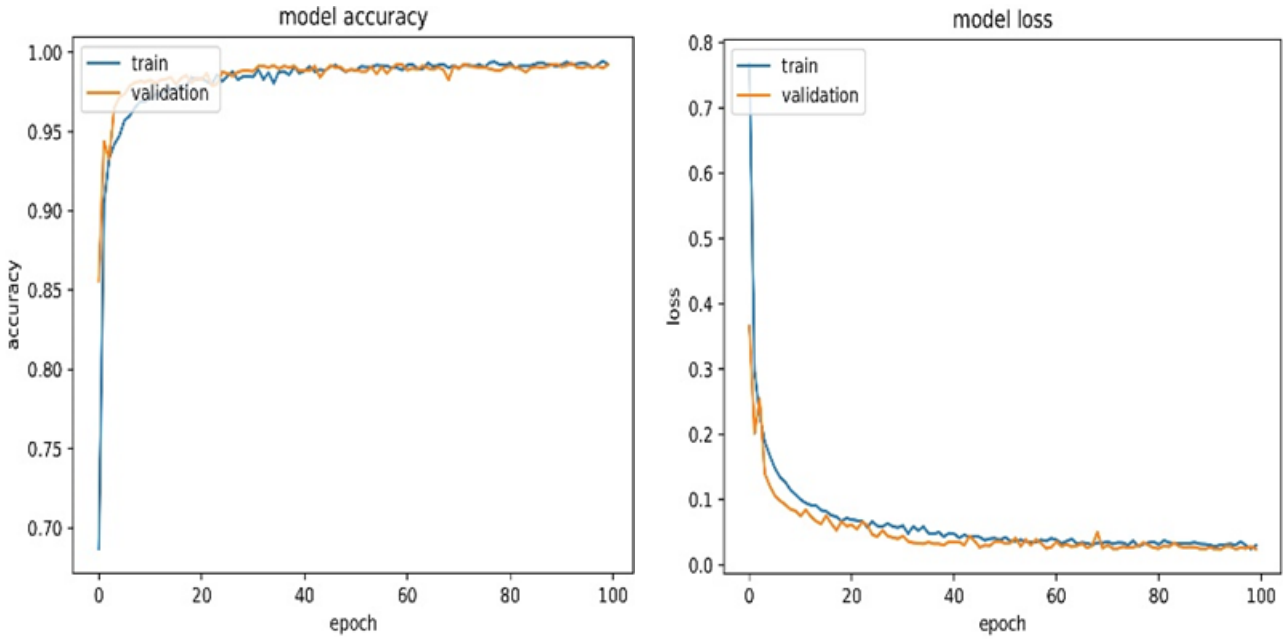

Figure 3. The InceptionV3 model's training and validation accuracy and loss curves

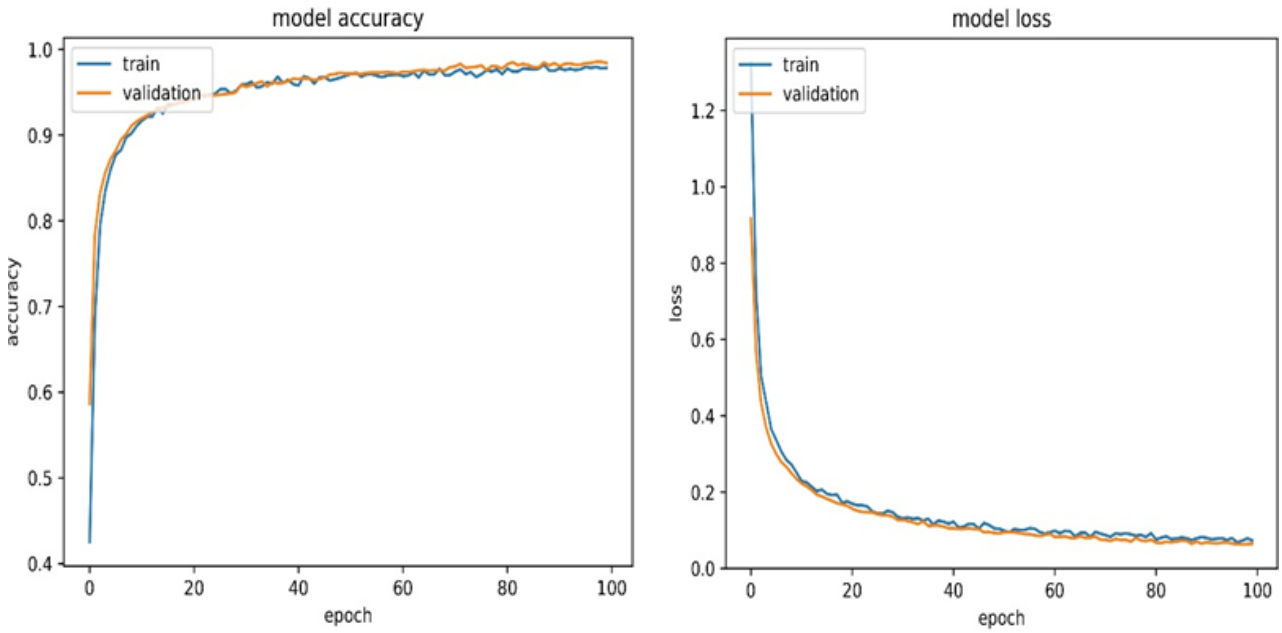

Figure 4. The ResNet50V2 model's training and validation accuracy and loss curves

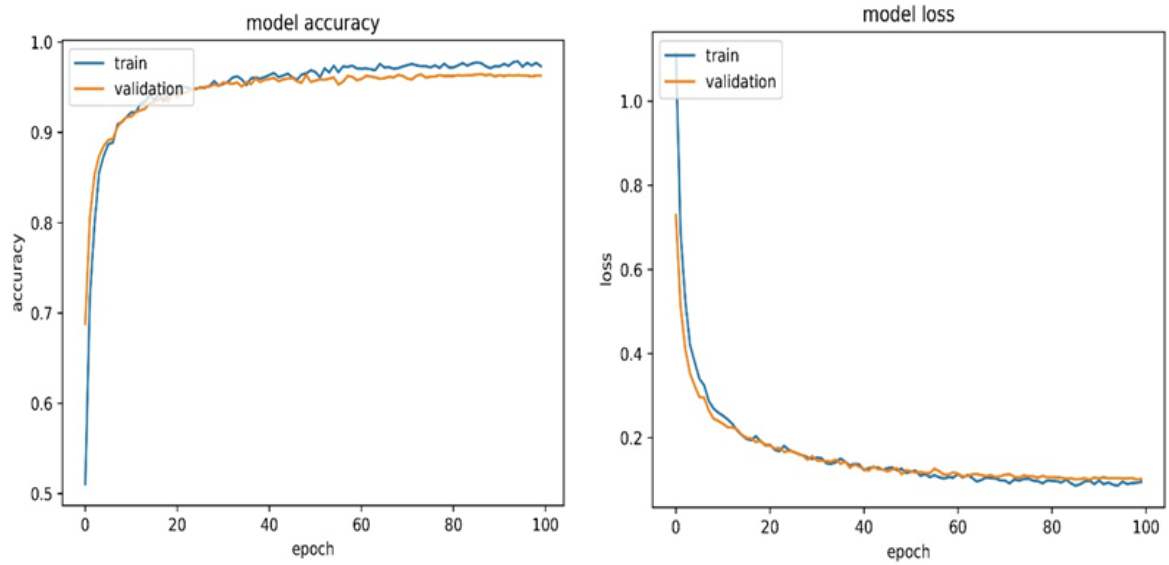

Figure 5. The ResNet101V2 model's training and validation accuracy and loss curves

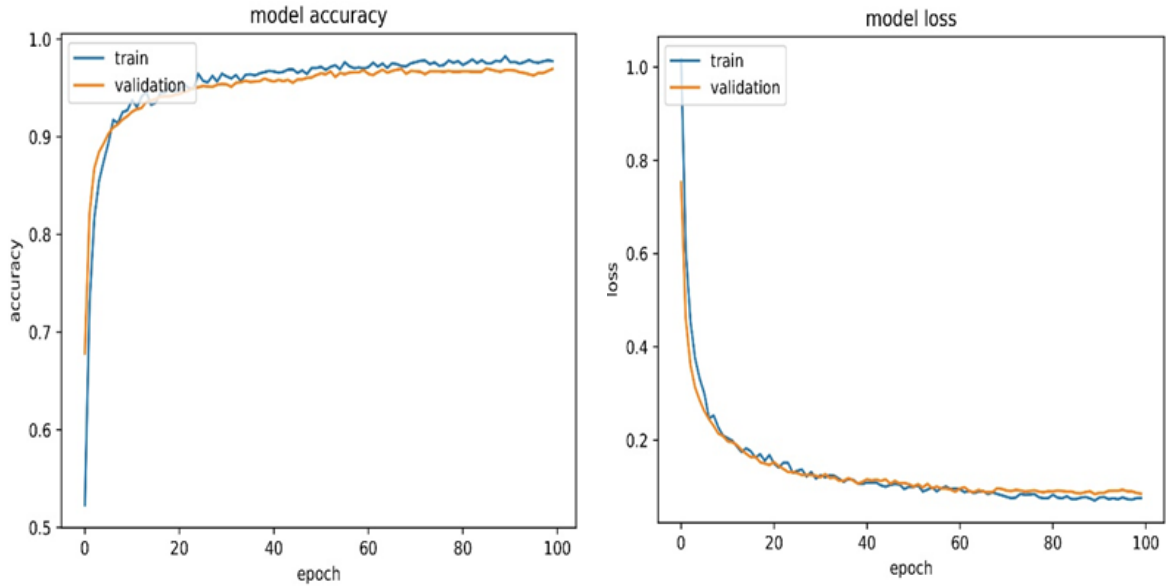

Figure 6. The ResNet152 model's training and validation accuracy and loss curves

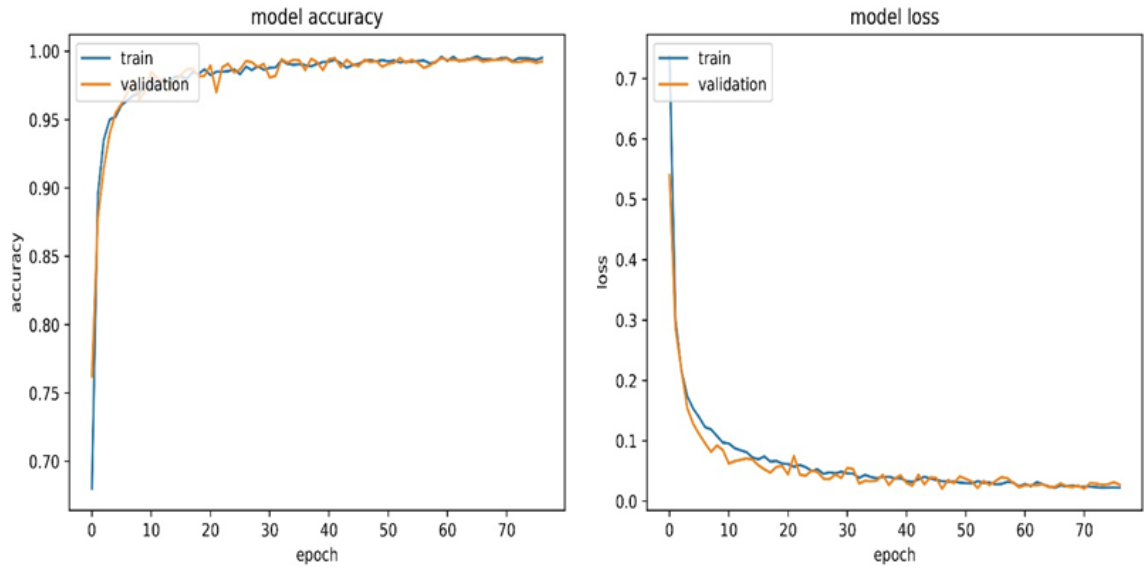

Figure 7. The DensNet121 model's training and validation accuracy and loss curves

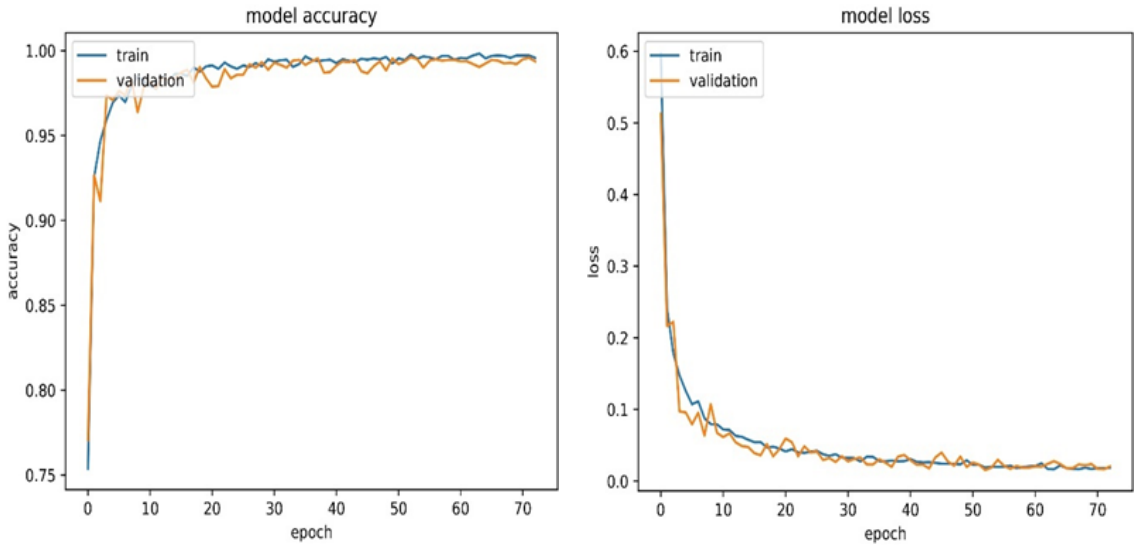

Figure 8. The DenseNet201 model's training and validation accuracy and loss curves

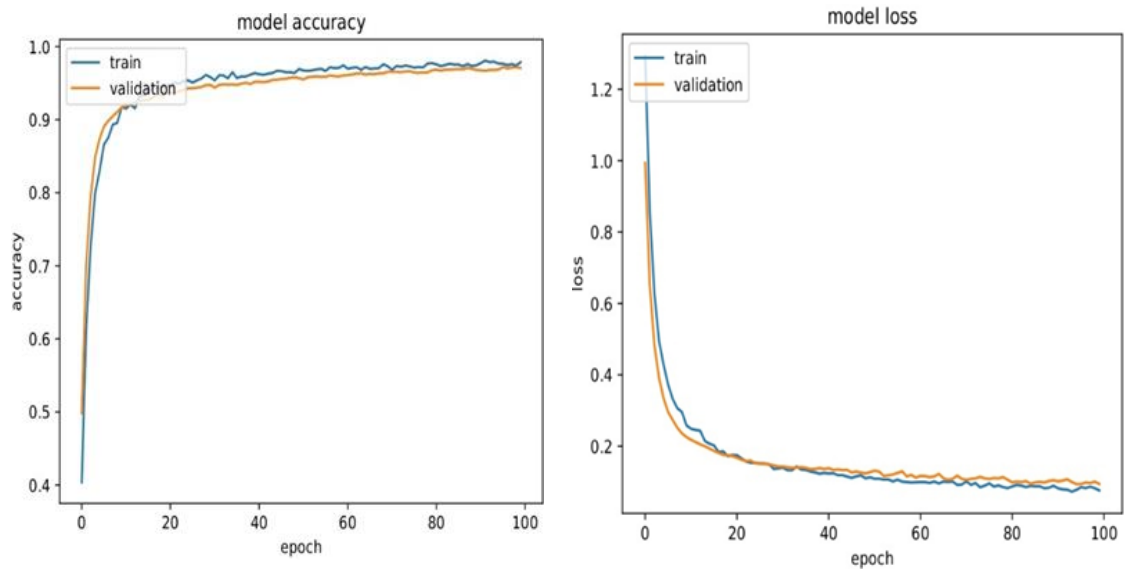

Figure 9. The MobileNet model's training and validation accuracy and loss curves

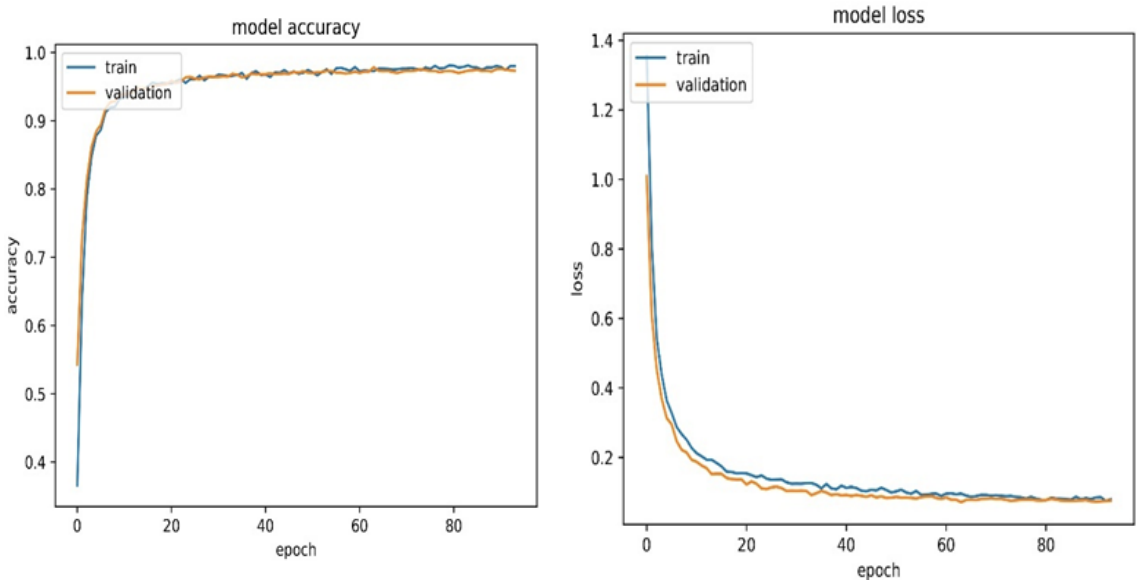

Figure 10. The MobileNetv2 model's training and validation accuracy and loss curves

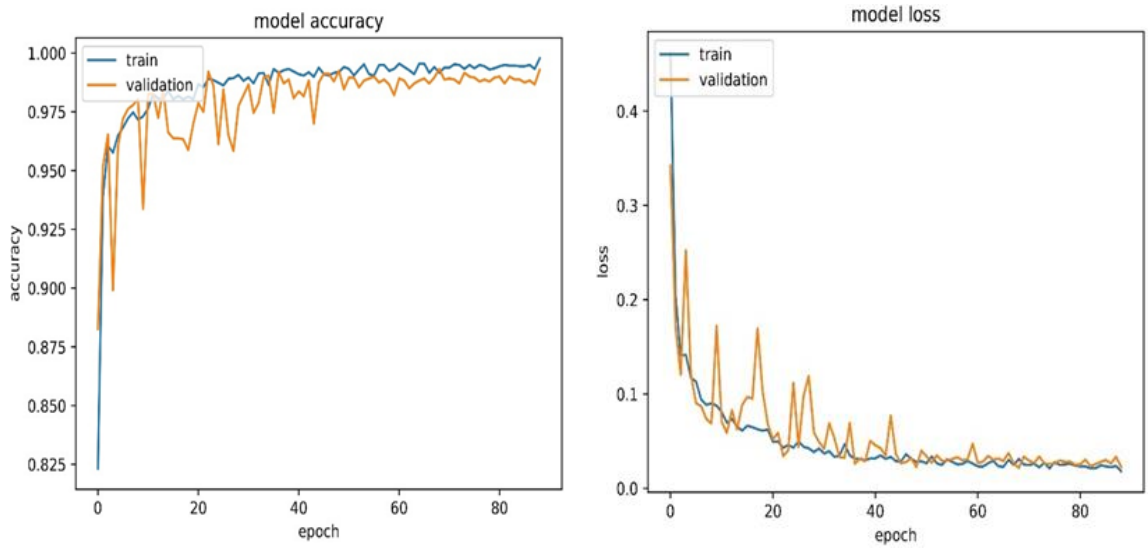

Figure 11. The Xception model's training and validation accuracy and loss curves

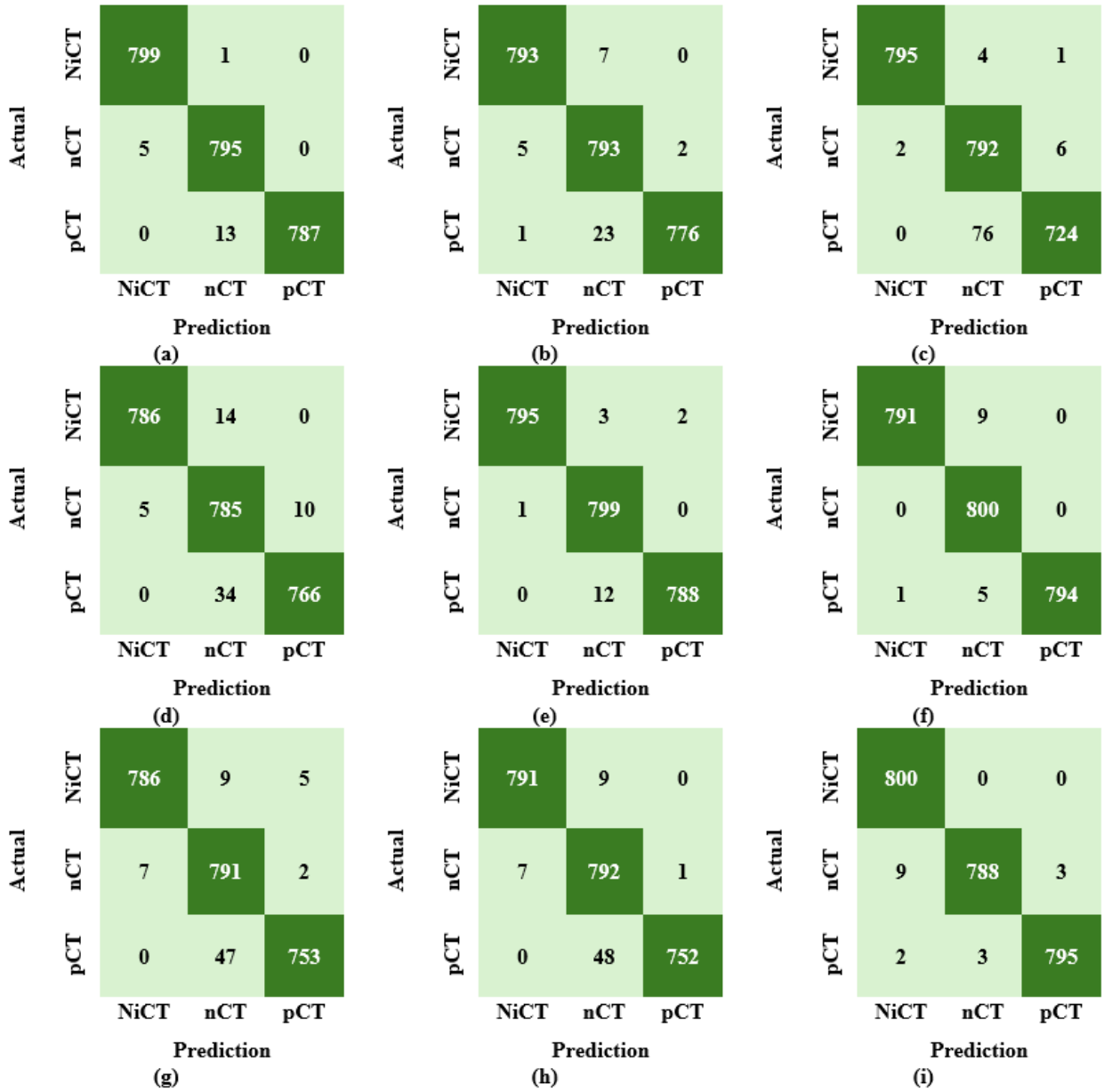

Figure 12. Confusion matrices obtained for different CNN models: (a) InceptionV3, (b) ResNet50V2, (c) ResNet101V2, (d) ResNet152V2, (e) DenseNet121, (f) DenseNet201, (g) MobileNet, (h) MobileNetV2, (i) Xception

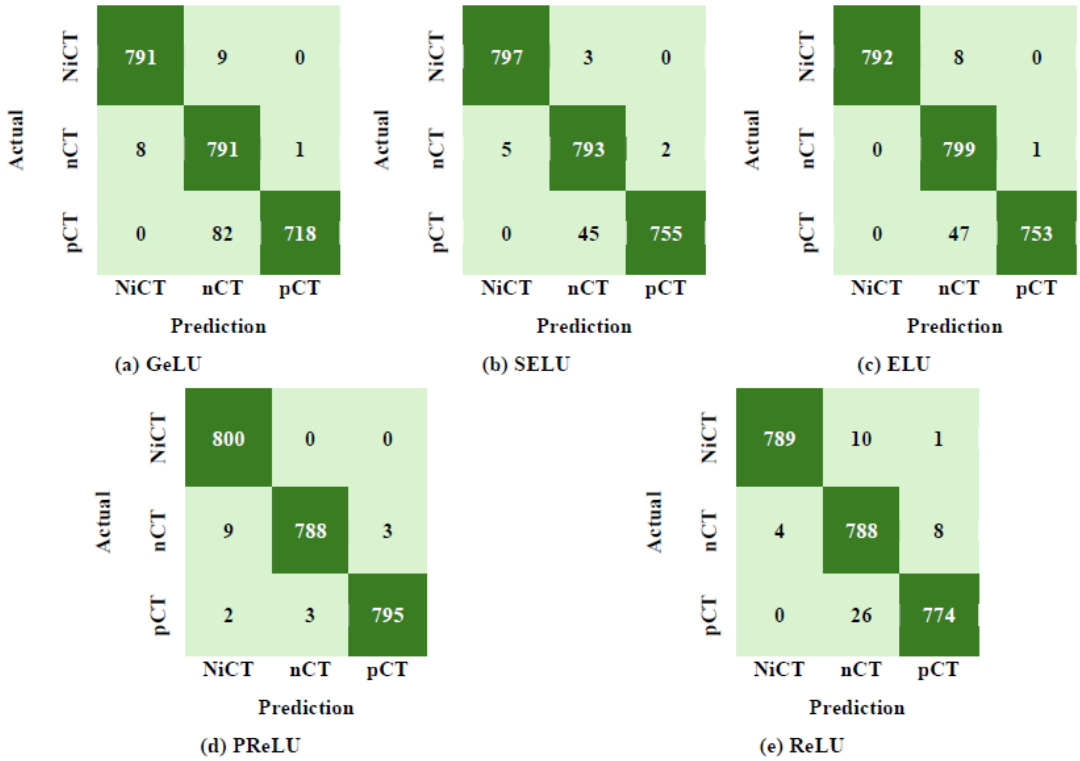

Figure 13. Confusion matrices obtained ResNet101V2 After Applying different activation functions: (a, b, c, d, e)

Figure 15 illustrates the application of the DenseNet121 architecture to external CT images for identifying COVID-19 cases and accurately localizing the affected regions [51, 52]. The DenseNet121 architecture correctly classified the images as COVID-19 and utilized Grad-CAM to visualize the disease-related areas. Notably, the model ignored any labels embedded within the images and focused solely on detecting the pathological regions, as indicated by the prominent red activation areas in COVID-19 cases. These experiments demonstrate the effectiveness of the proposed methodology in learning COVID-19–specific visual features and accurately identifying CT images from sources outside the training datasets.

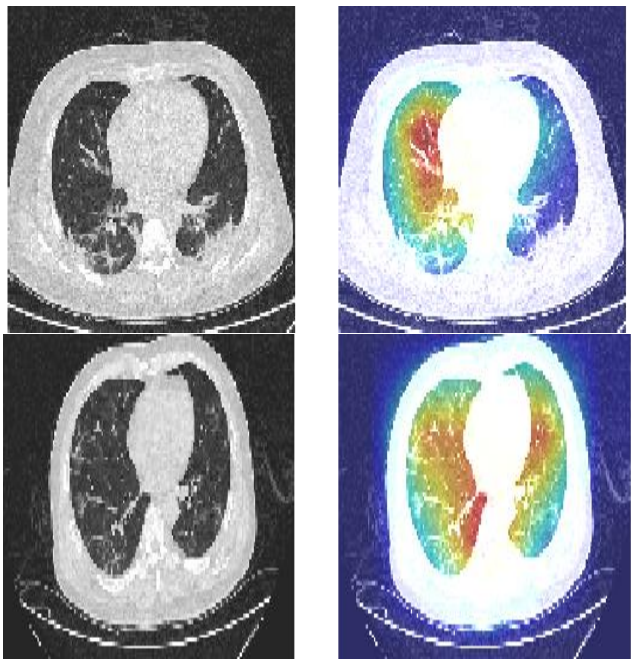

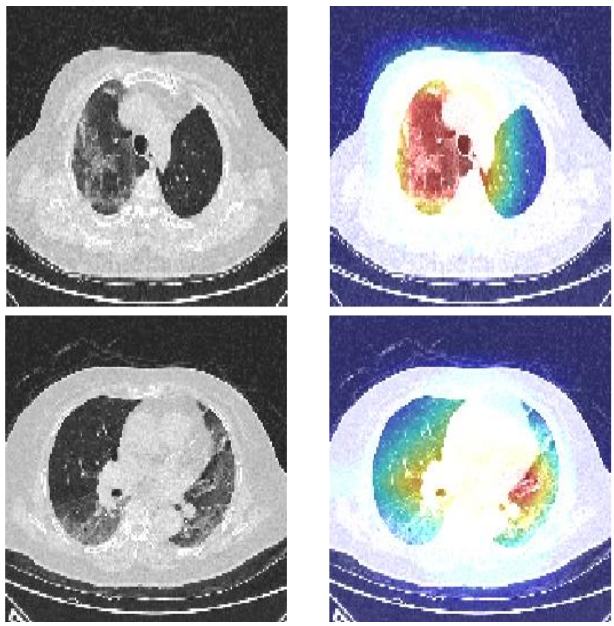

Figure 14. Grad-CAM visualizations showing a view of accurately classifying CT images from the COVID-19 dataset, with key regions identified for judging by DenseNet121

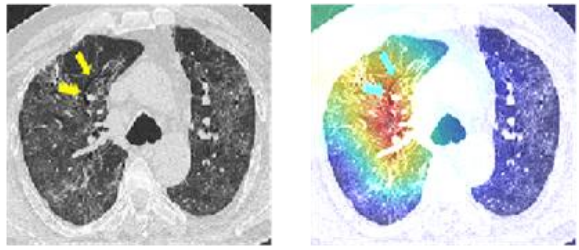

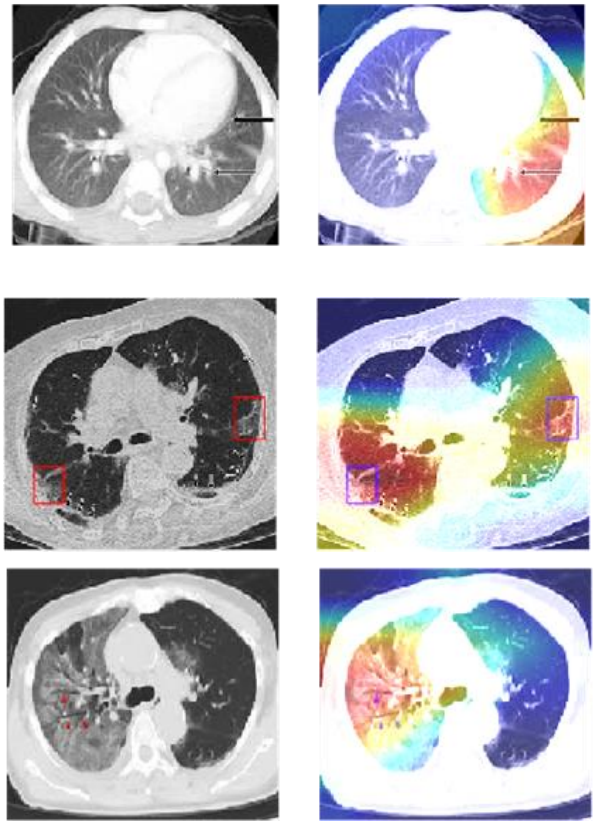

Figure 15. Grad-CAM visualization of CT images from external sources [51, 52]

6. CONCLUSIONS

We suggested a transfer learning method for CT-based COVID-19 identification using a sizable dataset of CTs divided into three classes, including pCT, NICT, and nCT images. The suggested method compared the performance of several well-designed pretrained CNN architectures and refined them. The deep network architectures include DenseNet121, DenseNet201, Xception, InceptionV3, MobileNetV2, MobileNet, ResNet50V2, ResNet152V2, and ResNet101v2, which are evaluated in automatically detecting COVID-19 from chest CTs. The obtained results demonstrated promising results with an accuracy, recall, precision, and F1-score of 99%, indicating the effective use of deep transfer learning as a tool for recognizing COVID-19 from CTs. Moreover, the effective impact of applying different activation functions on model performance was evaluated. Even though using different activation functions achieved better performance for some models, such as MobileNetV2 and ResNet152V2, the choice of activation function should be guided by the specific characteristics of the dataset, the architecture of the CNN, and the desired performance metrics. While DL-based methods have revealed satisfactory results for detecting COVID-19 from CT scans, they are not without limitations and should be implemented in conjunction with different diagnostic tools. Further research is needed to develop practical and reliable diagnostic tools for COVID-19.

ACKNOWLEDGMENT

Princess Nourah bint Abdulrahman University Researchers Supporting Project number (PNURSP2026R747), Princess Nourah bint Abdulrahman University, Riyadh, Saudi Arabia.

REFERENCES

[1] Ghinai, I., McPherson, T.D., Hunter, J.C., Kirking, H.L., et al. (2020). First known person-to-person transmission of severe acute respiratory syndrome coronavirus 2 (SARS-CoV-2) in the USA. The Lancet, 395(10230): 1137-1144. http://doi.org/10.1016/S0140-6736(20)30607-3

[2] Alshazly, H., Linse, C., Barth, E., Martinetz, T. (2021). Explainable COVID-19 detection using chest CT scans and deep learning. Sensors, 21(2): 455. http://doi.org/10.3390/s21020455

[3] Premamayudu, B., Bhuvaneswari, C. (2022). Covid-19 automatic detection from CT Images through transfer learning. International Journal of Image, Graphics and Signal Processing, 14(5): 84-95. http://doi.org/10.5815/ijigsp.2022.05.07

[4] Apostolopoulos, I.D., Mpesiana, T.A. (2020). Covid-19: Automatic detection from x-ray images utilizing transfer learning with convolutional neural networks. Physical and Engineering Sciences in Medicine, 43: 635-640. http://doi.org/10.1007/s13246-020-00865-4

[5] Hamza, A., Khan, M.A., Wang, S.H., Alhaisoni, M., Alharbi, M., Hussein, H.S., Alshazly, H., Kim, Y.J., Cha, J. (2022). COVID-19 classification using chest X-ray images based on fusion-assisted deep Bayesian optimization and Grad-CAM visualization. Frontiers in Public Health, 10(2022): 1046296. https://doi.org/10.3389/fpubh.2022.1046296

[6] Zheng, C., Deng, X., Fu, Q., Zhou, Q., Feng, J., Ma, H., Liu, W., Wang, X. (2020). Deep learning-based detection for COVID-19 from chest CT using weak label. MedRxiv, 2020-03. https://doi.org/10.1101/2020.03.12.20027185

[7] Kumar, R., Khan, A.A., Kumar, J., Golilarz, N.A., Zhang, S., Ting, Y., Zheng, C., Wang, W. (2021). Blockchain-federated-learning and deep learning models for covid-19 detection using CT imaging. IEEE Sensors Journal, 21(14): 16301-16314. http://doi.org/10.1109/JSEN.2021.3076767

[8] Rohila, V.S., Gupta, N., Kaul, A., Sharma, D.K. (2021). Deep learning assisted COVID-19 detection using full CT-scans. Internet of Things, 14: 100377. http://doi.org/10.1016/j.iot.2021.100377

[9] Song, Y., Zheng, S., Li, L., Zhang, X., Zhang, X., Huang, Z., Chen, J., Wang, R., Zhao, H., Chong, Y., Shen, J. (2021). Deep learning enables accurate diagnosis of novel coronavirus (COVID-19) with CT images. IEEE/ACM Transactions on Computational Biology and Bioinformatics, 18(6): 2775-2780. http://doi.org/10.1109/TCBB.2021.3065361

[10] Alshazly, H., Linse, C., Abdalla, M., Barth, E., Martinetz, T. (2021). COVID-Nets: Deep CNN architectures for detecting COVID-19 using chest CT scans. PeerJ Computer Science, 7: e655. http://doi.org/10.7717/peerj-cs.655

[11] Wang, S., Kang, B., Ma, J., Zeng, X., Xiao, M., Guo, J., Cai, M., Yang, J., Li, Y., Meng, X., Xu, B. (2021). A deep learning algorithm using CT images to screen for Corona Virus Disease (COVID-19). European

Radiology, 31: 6096-6104. http://doi.org/10.1007/s00330-021-07715-1
[12] Li, L., Qin, L., Xu, Z., Yin, Y., Wang, X., Kong, B., Bai, J., Lu, Y., Fang, Z., Song, Q., Cao, K. (2020). Using artificial intelligence to detect COVID-19 and community-acquired pneumonia based on pulmonary CT: Evaluation of the diagnostic accuracy. Radiology, 296(2): E65-E71. http://doi.org/10.1148/radiol.2020200905
[13] Kini, A.S., Gopal Reddy, A.N., Kaur, M., Satheesh, S., Singh, J., Martinetz, T., Alshazly, H. (2022). Ensemble deep learning and internet of things-based automated COVID-19 diagnosis framework. Contrast Media & Molecular Imaging, 2022(1): 7377502. http://doi.org/10.1155/2022/7377502
[14] Hamza, A., Khan, M.A., Wang, S.H., Alqahtani, A., Alsubai, S., Binbusayyis, A., Hussein, H.S., Martinetz, T.M., Alshazly, H. (2022). COVID-19 classification using chest X-ray images: A framework of CNN-LSTM and improved max value moth flame optimization. Frontiers in Public Health, 10: 948205. https://doi.org/10.3389/fpubh.2022.948205
[15] Akl, A.A., Hosny, K.M., Fouda, M.M., Salah, A. (2023). A hybrid CNN and ensemble model for COVID-19 lung infection detection on chest CT scans. PLoS One, 18(3): e0282608. http://doi.org/10.1371/journal.pone.0282608
[16] Lowe, D.G. (2004). Distinctive image features from scale-invariant keypoints. International Journal of Computer Vision, 60: 91-110. http://doi.org/10.1023/B:VISI.0000029664.99615.94
[17] Kanjanasurat, I., Tenghongsakul, K., Purahong, B., Lasakul, A. (2023). CNN–RNN network integration for the diagnosis of COVID-19 using chest X-ray and CT images. Sensors, 23(3): 1356. http://doi.org/10.3390/s23031356
[18] Zhang, K., Liu, X., Shen, J., Li, Z., Sang, Y., Wu, X., Zha, Y., Liang, W., Wang, C., Wang, K., Ye, L. (2020). Clinically applicable AI system for accurate diagnosis, quantitative measurements, and prognosis of COVID-19 pneumonia using computed tomography. Cell, 181(6): 1423-1433. http://doi.org/10.1016/j.cell.2020.04.045
[19] Chowdhury, M.E., Rahman, T., Khandakar, A., Mazhar, R., Kadir, M.A., Mahbub, Z.B., Islam, K.R., Khan, M.S., Iqbal, A., Al Emadi, N., Reaz, M.B.I. (2020). Can AI help in screening viral and COVID-19 pneumonia? IEEE Access, 8: 132665-132676. http://doi.org/10.1109/ACCESS.2020.3010287
[20] Cohen, J.P., Morrison, P., Dao, L., Roth, K., Duong, T.Q., Ghassemi, M. (2020). Covid-19 image data collection: Prospective predictions are the future. arXiv preprint arXiv:2006.11988. http://doi.org/10.59275/j.melba.2020-48g7
[21] Sahin, M.E., Ulutas, H., Yuce, E., Erkoc, M.F. (2023). Detection and classification of COVID-19 by using faster R-CNN and mask R-CNN on CT images. Neural Computing and Applications, 35(18): 13597-13611. http://doi.org/10.1007/s00521-023-08450-y
[22] Joshi, A.M., Nayak, D.R., Das, D., Zhang, Y. (2023). LiMS-Net: A lightweight multi-scale CNN for COVID-19 detection from chest CT scans. ACM Transactions on Management Information Systems, 14(1): 1-17. http://doi.org/10.1145/3551647
[23] Soares, E., Angelov, P., Biaso, S., Froes, M.H., Abe, D.K. (2020). SARS-CoV-2 CT-scan dataset: A large dataset of real patients CT scans for SARS-CoV-2 identification. MedRxiv, 2020-04. https://doi.org/10.1101/2020.04.24.20078584
[24] Sejuti, Z.A., Islam, M.S. (2023). A hybrid CNN–KNN approach for identification of COVID-19 with 5-fold cross validation. Sensors International, 4: 100229. http://doi.org/10.1016/j.sintl.2023.100229
[25] Afif, M., Ayachi, R., Said, Y., Atri, M. (2023). Deep learning-based technique for lesions segmentation in CT scan images for COVID-19 prediction. Multimedia Tools and Applications, 82(17): 26885-26899. http://doi.org/10.1007/s11042-023-14941-w
[26] Gunraj, H., Wang, L., Wong, A. (2020). COVIDNet-CT: A tailored deep convolutional neural network design for detection of COVID-19 cases from chest CT images. Frontiers in Medicine, 7: 608525. http://doi.org/10.3389/fmed.2020.608525
[27] Riyadi, S., Damarjati, C., Khotimah, S., Ishak, A.J. (2024). Optimization of the VGG deep learning model performance for COVID-19 detection using CT-scan images. Register: Scientific Journals of Information System Technology, 10(1): 91-101. http://doi.org/10.26594/register.v10i1.3598
[28] Maurya, P., Kushwaha, A., Khare, A., Prakash, O. (2024). Balancing accuracy and efficiency: A lightweight deep learning model for COVID 19 detection. Engineering Applications of Artificial Intelligence, 136: 108999. http://doi.org/10.1016/j.engappai.2024.108999
[29] Roy, M., Baruah, U., Varma, V. (2024). TransDL: A transfer learning-based concatenated model for COVID-19 identification and analysis of posteroanterior chest X-ray images. Multimedia Tools and Applications, 83(11): 33421-33443. http://doi.org/10.1007/s11042-023-16825-5
[30] Kermany, D.S., Goldbaum, M., Cai, W., Valentim, C.C., Liang, H., Baxter, S.L., McKeown, A., Yang, G., Wu, X., Yan, F., Dong, J. (2018). Identifying medical diagnoses and treatable diseases by image-based deep learning. Cell, 172(5): 1122-1131. http://doi.org/10.1016/j.cell.2018.02.010
[31] Echtioui, A., Ayed, Y.B. (2024). Automated detection of COVID-19 based on transfer learning. Multimedia Tools and Applications, 83(11): 33731-33751. http://doi.org/10.1007/s11042-023-17023-z
[32] Agrawal, S., Honnakasturi, V., Nara, M., Patil, N. (2023). Utilizing deep learning models and transfer learning for COVID-19 detection from X-ray images. SN Computer Science, 4(4): 326. http://doi.org/10.1007/s42979-022-01655-3
[33] Madhavi, K.R., Suneetha, K., Raju, K.S., Kora, P., Madhavi, G., Kallam, S. (2023). Detection of COVID 19 using X-ray images with fine-tuned transfer learning. Journal of Scientific & Industrial Research, 82(2): 241-248. http://doi.org/10.56042/jsir.v82i2.70216
[34] Zhao, W., Jiang, W., Qiu, X. (2021). Deep learning for COVID-19 detection based on CT images. Scientific Reports, 11(1): 14353. http://doi.org/10.1038/s41598-021-93832-2
[35] Subramanian, N., Elharrouss, O., Al-Maadeed, S., Chowdhury, M. (2022). A review of deep learning-based detection methods for COVID-19. Computers in Biology and Medicine, 143: 105233. http://doi.org/10.1016/j.compbiomed.2022.105233

[36] Gürsoy, E., Kaya, Y. (2023). An overview of deep learning techniques for COVID-19 detection: Methods, challenges, and future works. Multimedia Systems, 29(3): 1603-1627. http://doi.org/10.1007/s00530-023-01083-0

[37] Hasan, M.K., Alam, M.A., Dahal, L., Roy, S., Wahid, S.R., Elahi, M.T.E., Martí, R., Khanal, B. (2022). Challenges of deep learning methods for COVID-19 detection using public datasets. Informatics in Medicine Unlocked, 30: 100945. http://doi.org/10.1016/j.imu.2022.100945

[38] Alaufi, R., Kalkatawi, M., Abukhodair, F. (2024). Challenges of deep learning diagnosis for COVID-19 from chest imaging. Multimedia Tools and Applications, 83(5): 14337-14361. http://doi.org/10.1007/s11042-023-16017-1

[39] Khan, W.Z., Azam, F., Khan, M.K. (2022). Deep-learning-based COVID-19 detection: Challenges and future directions. IEEE Transactions on Artificial Intelligence, 4(2): 210-228. http://doi.org/10.1109/TAI.2022.3224097

[40] Szegedy, C., Vanhoucke, V., Ioffe, S., Shlens, J., Wojna, Z. (2016). Rethinking the inception architecture for computer vision. In Proceedings of the IEEE Conference on Computer Vision and Pattern Recognition (CVPR), Las Vegas, NV, USA, pp. 2818-2826. http://doi.org/10.1109/CVPR.2016.308

[41] He, K., Zhang, X., Ren, S., Sun, J. (2016). Deep residual learning for image recognition. In Proceedings of the IEEE Conference on Computer Vision and Pattern Recognition (CVPR), Las Vegas, NV, USA, pp. 770-778. http://doi.org/10.1109/CVPR.2016.90

[42] Huang, G., Liu, Z., Van Der Maaten, L., Weinberger, K.Q. (2017). Densely connected convolutional networks. In Proceedings of the IEEE Conference on Computer Vision and Pattern Recognition (CVPR), Honolulu, HI, USA, pp. 4700-4708. http://doi.org/10.1109/CVPR.2017.243

[43] Sandler, M., Howard, A., Zhu, M., Zhmoginov, A., Chen, L.C. (2018). Mobilenetv2: Inverted residuals and linear bottlenecks. In Proceedings of the IEEE Conference on Computer Vision and Pattern Recognition (CVPR), Salt Lake City, UT, USA, pp. 4510-4520. http://doi.org/10.1109/CVPR.2018.00474

[44] Chollet, F. (2017). Xception: Deep learning with depthwise separable convolutions. In Proceedings of the IEEE Conference on Computer Vision and Pattern Recognition (CVPR), Honolulu, HI, USA, pp. 1251-1258. http://doi.org/10.1109/CVPR.2017.195

[45] Ning, W., Lei, S., Yang, J., Cao, Y., Jiang, P., Yang, Q., Zhang, J., Wang, X., Chen, F., Geng, Z., Xiong, L. (2020). Open resource of clinical data from patients with pneumonia for the prediction of COVID-19 outcomes via deep learning. Nature Biomedical Engineering, 4(12): 1197-1207. http://doi.org/10.1038/s41551-020-00633-5

[46] Clevert, D.A., Unterthiner, T., Hochreiter, S. (2015). Fast and accurate deep network learning by exponential linear units (ELU s). arXiv preprint arXiv:1511.07289. https://doi.org/10.48550/arXiv.1511.07289

[47] Klambauer, G., Unterthiner, T., Mayr, A., Hochreiter, S. (2017). Self-normalizing neural networks. In 31st Conference on Neural Information Processing Systems (NIPS 2017), Long Beach, CA, USA. pp. 1-10. https://doi.org/10.48550/arXiv.1706.02515

[48] Maas, A.L., Hannun, A.Y., Ng, A.Y. (2013). Rectifier nonlinearities improve neural network acoustic models. In Proceedings of the 30th International Conference on Machine Learning, Atlanta, Georgia, USA, pp. 1-6.

[49] Hendrycks, D., Gimpel, K. (2016). Gaussian error linear units (GELU s). arXiv preprint arXiv:1606.08415. https://doi.org/10.48550/arXiv.1606.08415

[50] He, K., Zhang, X., Ren, S., Sun, J. (2015). Delving deep into rectifiers: Surpassing human-level performance on ImageNet classification. In Proceedings of the IEEE International Conference on Computer Vision (ICCV), Santiago, Chile, pp. 1026-1034. http://doi.org/10.1109/ICCV.2015.123

[51] Ye, Z., Zhang, Y., Wang, Y., Huang, Z., Song, B. (2020). Chest CT manifestations of new coronavirus disease 2019 (COVID-19): A pictorial review. European Radiology, 30(8): 4381-4389. http://doi.org/10.1007/s00330-020-06801-0

[52] Palmisano, A., Scotti, G.M., Ippolito, D., Morelli, M.J., Vignale, D., Gandola, D., Sironi, S., De Cobelli, F., Ferrante, L., Spessot, M., Tonon, G. (2021). Chest CT in the emergency department for suspected COVID-19 pneumonia. La Radiologia Medica, 126(3): 498-502. http://doi.org/10.1007/s11547-020-01302-y